FARADAY

Promotion by strontium fluoride of neodymium oxide catalysis of the oxidative coupling of methane

Ruiqiang Long*† and Huilin Wan

Department of Chemistry and State Key Laboratory for Physical Chemistry of the Solid Surface, Xiamen University, Xiamen, 361005, People's Republic of China

Catalytic performance measurements showed that CH_4 conversion and C_2 selectivity were higher over SrF_2/Nd_2O_3 catalyst than over pure Nd_2O_3 for the oxidative coupling of methane (OCM). XRD indicated that there was some exchange of F^- and O^{2-}, leading to the formation of tetragonal and rhombohedral NdOF phases during the catalyst preparation. After a certain amount of SrF_2 was added to Nd_2O_3, the increase in surface basicity and conductivity, as well as the role of F^- on the dispersion of surface active sites, would be favourable to a decrease in the secondary deep oxidation of methyl radicals and C_2 hydrocarbons, giving improved C_2 selectivity. Since there is a certain correlation between methane conversion and C_2 selectivity for an oxygen-limited OCM reaction, methane conversion is also expected to increase with the increase in C_2 selectivity.

OCM to C_2 hydrocarbons is an attractive means of using the abundant natural-gas resource. Since Otsuka *et al.*[1] reported that rare earth oxides (REO), with the exception of Ce, Pr, and Tb oxides, exhibit very high C_2 selectivity for OCM under the condition of extremely high CH_4/O_2 ratio, REO, either alone or in combination with alkali- or alkaline-earth-metal oxides or carbonates, have been extensively studied as OCM catalysts.[2–8] From previous work, it has been generally accepted that the major reaction path of the OCM reaction is as follows: a methane molecule reacts with a surface oxygen species to produce a gaseous methyl radical, which may then couple with a second methyl radical in the gas phase to give ethane; further dehydrogenation of ethane to form ethene takes place in the gas phase or on the surface of catalyst.[2,3,9–11] Together with this major reaction path, methyl radicals and C_2 hydrocarbons also have a chance of being deeply oxidized to carbon dioxide or monoxide (CO_x) on the catalyst surface, so it is necessary to minimize the secondary deep oxidation reaction in order to get a good C_2 selectivity and yield.

Many investigators have found that the catalytic performance, especially the selectivity to ethene, can be significantly improved by chlorine, present either in the form of a chloride component built into the catalyst or as a volatile chlorinated compound (organic or inorganic) in the reactant feed.[3,7,8] Considering that metal fluorides (especially alkaline-earth-metal fluorides) are usually more stable than the corresponding chlorides, and that F^- ($r = 0.133$ nm) and O^{2-} ($r = 0.132$ nm) have similar ionic radii so that anionic exchange between fluoride and oxide may easily take place (leading to the formation of lattice defects, such as anionic vacancies that are requisites for the adsorption and activation of O_2 over the compound catalysts with stable cationic valences), we have developed a new series of metal fluoride (mainly alkaline-earth-metal fluoride) promoted REO catalysts in recent years. These catalysts (*e.g.* SrF_2–La_2O_3, SrO–LaF_3, BaF_2–CeO_2, Cs_2O–CeF_3–CeO_2) showed good catalytic performance in OCM and in the oxidative dehydrogenation of light alkanes (C_2H_6 and C_3H_8).[12,13] In previous work, we found that, when metal fluoride was added to oxides, partial substitution of cations and/or anions occurred. In order to understand clearly the nature of the promoting effect of alkaline-earth-metal fluoride, we also investigated the catalytic performance for the OCM reaction over different alkaline-earth-metal fluoride promoted neodymium oxide catalysts. The results showed that CH_4 conversion and C_2 selectivity over these alkaline-earth-metal fluoride promoted Nd_2O_3 catalysts were apparently better than over pure Nd_2O_3 and that SrF_2 was the best promoter among these alkaline-earth-metal fluorides, hence we have focused on the SrF_2–Nd_2O_3 catalyst in this study. The surface properties (*e.g.* specific surface area, surface element composition, surface basicity) and bulk properties (*e.g.* bulk composition and structure, and conductivity) of the SrF_2-promoted Nd_2O_3 catalyst were also studied and compared with pure Nd_2O_3. The reason that surface basicity and conductivity were selected for study is that these two properties have been considered to be two fundamental characteristics of a good OCM catalyst.[8] The relationship between the physicochemical properties and catalytic performance of the catalysts is discussed. The results showed that SrF_2 modified the surface and bulk properties of Nd_2O_3, leading to an increase in surface basicity and conductivity. This would favour a decrease in the secondary deep oxidation of methyl radicals and C_2 hydrocarbons, and result in an improvement in C_2 selectivity. Moreover, the increase in methane conversion is attributed to the improvement in C_2 selectivity, because there is a certain relationship between methane conversion and C_2 selectivity for an oxygen-limited OCM reaction.

Experimental

Preparation and evaluation of catalyst

Each catalyst sample was prepared by the method of grinding and calcination, as described elsewhere.[13] Different mole ratios of SrF_2–Nd_2O_3, CaF_2–Nd_2O_3, BaF_2–Nd_2O_3 and $Sr(NO_3)_2$–Nd_2O_3 were mixed and carefully ground into fine powder. The solid mixture was mixed with a certain amount of deionized water to form a paste, then dried at 393 K for 4 h and calcined at 1173 K for 6 h. The resulting solid was crushed and sieved to 40–60 mesh particles. The pure Nd_2O_3 and SrF_2 used for the catalytic performance evaluation were also treated similarly. The materials, such as Nd_2O_3 (99.95%), CaF_2 (98.5%), SrF_2 (>98%), BaF_2 (98.5%) and $Sr(NO_3)_2$ (99.5%), were obtained from Shanghai Chemicals Company.

The catalytic reaction was carried out in a fixed-bed quartz reactor, 5.0 mm id, with $CH_4/O_2 = 2$–8 (mole ratios, without

† Current address: Department of Chemical Engineering, University of Michigan, Ann Arbor, MI 48109-2136, USA.

dilution gas) with a flow rate of 66.7 ml min^{-1}; methane (99.99%) and oxygen (99.5%) were used without further purification. In each experimental run, 0.20 ml (unless otherwise indicated) of catalyst was used, and the effluent gas was analysed at room temperature with an on-line Shang Fen 102 GD gas chromatograph equipped with a thermal conductivity detector, with 5A molecular sieve column for O_2 and CO, and a GDX 502 column for CH_4, C_2H_4, C_2H_6 and CO_2. Water and hydrogen gas were also present but were not measured. Other details were as reported previously.[13]

To determine the fluorine loss after calcination and reaction, 20 mg of the fresh and used 50 mol.% SrF_2–Nd_2O_3 catalysts were weighed and dissolved in *ca.* 2 ml of 6 M nitric acid. The pH of the solution was then adjusted to 6–7 by adding a certain amount of 1.1 M CH_3CO_2Na solution. The solutions were then diluted to 50.00 ml in a volumetric flask. In each case, the concentration of F^- in the solution was determined by means of a calibrated fluoride-ion-selective electrode.[14] Based on the weight of the catalyst and the concentration of F^- in the solution, the content of fluorine in the catalyst (expressed as mg of F^- per gram of catalyst) was easily determined.

Catalyst characterization

The surface composition was analysed by means of X-ray photoelectron spectroscopy (XPS). Spectra were recorded on a VG ESCALAB 210 XPS/AES instrument at room temperature, with Mg-Kα as the excitation radiation. The catalyst samples were pressed into wafers (diameter, 10 mm) under a pressure of 100 kg cm^{-2} and were loaded onto a sample holder for XPS analysis. The base pressure of the XPS analysis chamber was *ca.* 7×10^{-11} Torr. All measured binding energies were calibrated with respect to the C 1s energy at 284.6 eV due to adventitious carbon. Eclipse 1.7T software was used to resolve the experimental spectra. The surface composition of the catalysts was estimated from peak areas using appropriate instrumental sensitivity factors.

The specific surface area of the catalyst was measured by the BET method with N_2 adsorption at 77 K on a Sorptmatic 1900 Carlo Erba instrument. A large quantity of catalyst (5.0 g) was used, in order to increase the precision of the measurement. Samples were outgassed at 523 K under vacuum (5×10^{-2} Torr) for 3 h before nitrogen adsorption. The specific surface areas of Nd_2O_3 and 50 mol.% SrF_2–Nd_2O_3 were 4.4 and 3.8 m^2 g^{-1}, respectively.

The basicity of the catalyst was measured by temperature-programmed desorption (TPD) of carbon dioxide (adsorbed at 300 K) in a quartz reactor from 300 to 1173 K at a linear heating rate of 20 K min^{-1} in a flow of helium (30 ml min^{-1}). Before the TPD experiment, the catalyst (0.2 g) packed in a quartz reactor was treated in a flow of helium at 1173 K for 30 min. The amount of carbon dioxide desorbed was determined with a gas chromatograph equipped with a thermal conductivity detector.

The bulk composition and structure of the catalyst were measured by XRD. The experiment was carried out at room temperature on a Rigaku Rotaflex D/Max-C system with Cu-Kα ($\lambda = 0.15406$ nm) radiation. The samples were loaded to a depth of 1 mm on a sample holder. XRD powder patterns were recorded in the range $2\theta = 20$–$70°$.

The conductivity was determined by measuring the specific resistance of the catalyst disk between two parallel platinum sheet electrodes in the frequency region 0.1–100 kHz on an M378 system. Before the measurement, the catalyst was pressed to a disk with a diameter of 13 mm and a thickness of 2.5–3 mm under a pressure of 4.5×10^3 kg cm^{-2} and calcined at 1173 K for 12 h. Platinum was then sprayed onto the surface of the sample under vacuum (10^{-2} Torr) in an IB-3 10N Coater instrument, in order to minimize the contact resistance between the platinum electrode and the sample. The sample was laid in a quartz cell and heated from room temperature to 1173 K in a flow of N_2 (20 ml min^{-1}). The resistance spectra were recorded at specified temperatures during the heating period. At each specified temperature, the temperature of the quartz cell was maintained constant for *ca.* 10 min, to ensure that the resistance measurement was conducted under thermostatic conditions.

Results and Discussion

Catalytic performance

The catalytic performances of the catalysts for OCM are summarized in Table 1. Over pure Nd_2O_3 catalyst, only 26.6–27.7% methane conversion and 36.3–42.7% C_2 selectivity were obtained in the temperature range 973–1073 K with a $CH_4/O_2 = 3/1$ and GHSV = 20 000 h^{-1}. Whereas, after the addition of a certain amount of SrF_2 (which alone showed almost no activity for OCM) to Nd_2O_3, and ignition at high temperature, methane conversion and C_2 selectivity, as well as the ethene/ethane ratio, increased under identical conditions. At the same time, the catalytic performance of 50 mol.% SrF_2–Nd_2O_3 catalyst was also found to be superior to that of 50 mol.% SrO-promoted Nd_2O_3 catalyst, indicating that strontium fluoride played a significant promoting role for OCM with Nd_2O_3 as host catalyst. A maximum C_2 yield of 19.6% could be obtained over 50 mol.% SrF_2–Nd_2O_3 catalyst at 1023 K, which was *ca.* 9% and 5% higher than over Nd_2O_3 and 50 mol.% SrO–Nd_2O_3 catalysts under the same conditions.

Table 1 Catalytic performance of catalysts for OCM

catalyst	T/K	conv. (%)		selectivity (%)					C_2 yield (%)
		CH_4	O_2	CO	CO_2	C_2H_4	C_2H_6	C_2	
SrF_2	1073	2.5	3.8	0	24.8	16.4	58.8	75.2	1.9
	1023	0.8	1.4	0	46.0	0	54.0	54	0.4
	973	no activity							
Nd_2O_3	1073	26.6	99.6	8.2	55.5	19.2	17.1	36.3	9.6
	1023	27.2	99.7	7.2	53.5	20.1	19.2	39.3	10.7
	973	27.7	99.7	5.8	51.5	21.7	21.0	42.7	11.8
50 mol.% SrO–Nd_2O_3	1073	28.8	99.3	4.1	47.7	27.4	20.8	48.2	13.9
	1023	29.4	99.1	4.1	45.8	27.8	22.3	50.1	14.7
	973	30.0	99.2	4.3	44.3	28.0	23.4	51.4	15.4
50 mol.% SrF_2–Nd_2O_3	1073	33.6	99.0	3.7	39.7	33.5	23.1	56.6	19.0
	1023	34.3	98.9	4.0	38.9	33.1	24.0	57.1	19.6
	973	33.7	98.7	5.1	39.9	30.4	24.5	54.9	18.5
	923	33.1	98.2	7.1	41.0	27.2	24.7	51.9	17.2

Conditions: $CH_4/O_2 = 3/1$ and GHSV = 20 000 h^{-1}.

Table 2 Catalytic performance of 50 mol.% MF_2–Nd_2O_3 (M = Ca, Sr, and Ba) catalysts

catalyst	conv. (%)		selectivity (%)					C_2 yield (%)
	CH_4	O_2	CO	CO_2	C_2H_4	C_2H_6	C_2	
CaF_2–Nd_2O_3	29.6	98.9	6.8	45.2	26.1	21.9	48.0	14.2
SrF_2–Nd_2O_3	34.3	98.9	4.0	38.9	33.1	24.0	57.1	19.6
BaF_2–Nd_2O_3	30.8	99.3	3.5	42.6	30.6	23.3	53.9	16.6

Conditions: T = 1023 K, CH_4/O_2 = 3/1, and GHSV = 20 000 h^{-1}.

Table 2 shows the catalytic performance over different alkaline-earth-metal fluoride promoted Nd_2O_3 catalysts at 1023 K. The methane conversion and C_2 selectivity were found to increase according to the sequence Ca < Ba < Sr, *i.e.* SrF_2 was the most effective promoter among the alkaline-earth-metal fluorides for the Nd_2O_3 catalyst in the OCM reaction.

As shown in Fig. 1, at 1023 K, methane conversion and C_2 selectivity increased with SrF_2 loading, reached a maximum at 33–50 mol.%, and then decreased as the loading increased further. Over 50 mol.% SrF_2–Nd_2O_3 catalyst, when the CH_4/O_2 ratio was increased from 2/1 to 8/1, the C_2 selectivity increased from 44.4% to 73.4%, with an accompanying decrease in CH_4 conversion from 41.5% to 17.7% at 1023 K (Fig. 2).

In the absence of catalyst, the conversion of methane was less than 0.7% at 923–1073 K with CH_4/O_2 = 3/1 and GHSV = 20 000 h^{-1}. This showed that the conversion of methane by its homogeneous oxidation with O_2 was negligibly small compared with OCM over the catalysts studied.

The catalytic performance of the 50 mol.% SrF_2–Nd_2O_3 catalyst with respect to time on stream indicated that CH_4 conversion and C_2 selectivity gradually decreased over a period of 30 h at 1023 K with CH_4/O_2 = 3/1 and GHSV = 20 000 h^{-1}, leading to a decrease in C_2 yield from 19.6% to 15.2%. The C_2 yield then remained almost unchanged for the following 15 h. The gradual change in the catalytic behaviour of the catalyst was accompanied by the loss of some F^- from the sample as HF. The analytical result showed that the content of fluorine in the fresh 50 mol.% SrF_2–Nd_2O_3 was 78.6 mg g^{-1}, which was smaller than that (82.2 mg g^{-1}) in the sample before calcination. After reacting for 45 h, the content fluorine in the catalyst decreased to 56.7 mg g^{-1}.

Over the catalysts studied (except for those with SrF_2 content exceeding 75 mol.%), the conversions of oxygen were more than 98%, indicating that OCM was carried out under an oxygen-limited condition. This makes it difficult to compare the real activity of these catalysts and the reason for the increase in methane conversion becomes complex as a result of doping the Nd_2O_3 host catalyst with strontium fluoride. It is interesting to note that, for almost all of the catalysts under the same methane-to-oxygen mole ratio, the higher the C_2 selectivity, the higher the methane conversion, under different conditions. For example, over 50 mol.% SrF_2–Nd_2O_3 catalyst, C_2 selectivity was found to increase at first, pass through a maximum, then decrease as the temperature increased from 923 to 1073 K, and the methane conversion varied with temperature in the same manner (Table 1). This phenomenon was also observed over other catalysts at different temperatures (Table 1). Hence, it is suggested that C_2 selectivity may have something to do with methane conversion for an oxygen-limited OCM reaction. According to the reaction equations:

$$CH_4 + 1/4O_2 = 1/2C_2H_6 + 1/2H_2O \quad (1)$$

$$CH_4 + 1/2O_2 = 1/2C_2H_4 + H_2O \quad (2)$$

$$CH_4 + 3/2O_2 = CO + 2H_2O \quad (3)$$

$$CH_4 + 2O_2 = CO_2 + 2H_2O \quad (4)$$

it is obvious that the amount of oxygen consumed in converting a definite amount of methane to ethene and ethane [eqn. (1) and (2)] is less than that used to convert the same amount

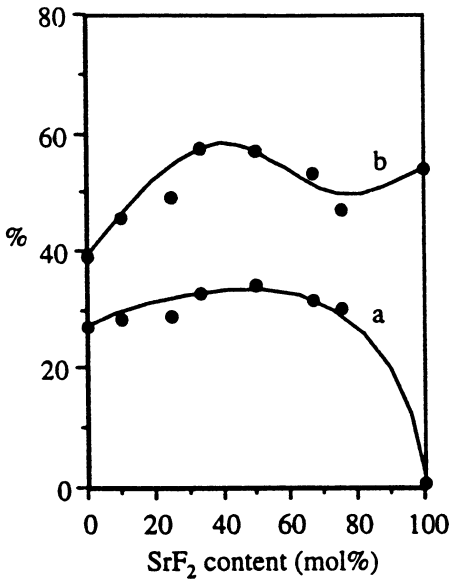

Fig. 1 Effect of SrF_2 content on (a) CH_4 conversion and (b) C_2 selectivity over SrF_2–Nd_2O_3 catalysts at 1023 K with GHSV = 20 000 h^{-1} and CH_4/O_2 = 3

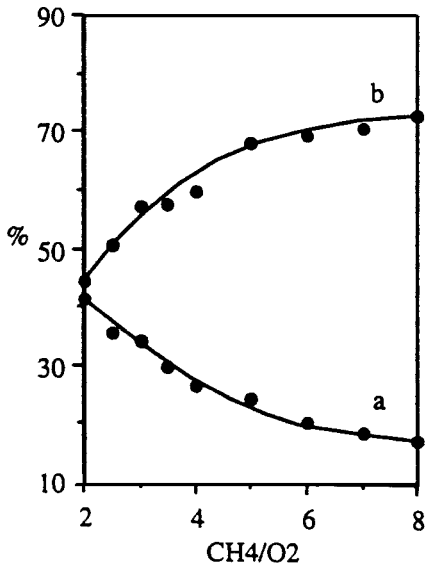

Fig. 2 Effect of CH_4/O_2 ratio on (a) CH_4 conversion and (b) C_2 selectivity over 50 mol.% SrF_2–Nd_2O_3 catalysts at 1023 K with GHSV = 20 000 h^{-1}

Table 3 Effect of the amount of catalyst on the catalytic performance

catalyst	volume /ml	conv. (%)		selectivity (%)					C_2 yield (%)
		CH_4	O_2	CO	CO_2	C_2H_4	C_2H_6	C_2	
Nd_2O_3	0.2	27.2	99.7	7.2	53.5	20.1	19.2	39.3	10.7
	0.1	27.5	99.8	10.4	49.9	20.9	18.8	39.7	10.9
	0.05	27.4	99.7	11.7	48.9	20.7	18.7	39.4	10.8
	0.02	28.0	99.6	14.9	44.8	20.3	20.0	40.3	11.2
50 mol.% SrF_2–Nd_2O_3	0.2	34.3	98.9	4.0	38.9	33.1	24.0	57.1	19.6
	0.1	33.9	99.7	4.9	38.6	32.1	24.4	56.5	19.2
	0.05	24.9	80.5	8.6	35.3	29.3	26.8	56.1	14.0
	0.02	14.0	38.0	12.3	37.0	15.8	34.9	50.7	7.1

Conditions: $T = 1023$ K, and $CH_4/O_2 = 3/1$ with a flow rate of 66.7 ml min^{-1}.

Table 4 Electron binding energies of the elements on the fresh catalysts

catalyst	E_b/eV				
	Nd $3d_{5/2}$	Sr $3d_{5/2}$	F 1s	O 1s	C 1s
Nd_2O_3	982.1	—	—	531.8, 530.7, 529.0	289.2, 284.6
50 mol.% SrF_2–Nd_2O_3	982.1	133.7	684.5	531.9, 530.9, 528.7	289.2, 284.6

of methane to CO_x [eqn. (3) and (4)]. For an oxygen-limited OCM reaction, there will be little oxygen left in the gas phase after the reactant flows over a short distance of catalyst bed, hence a large amount of methane can no longer be activated. Owing to the increase in C_2 selectivity as a result of adding strontium fluoride to Nd_2O_3, a smaller amount of oxygen would be used to convert the same amount of methane (mainly to C_2 products) over this catalyst than that over undoped Nd_2O_3 catalyst (mainly to CO_x), leading to the results that the reaction zone of the catalyst bed for the doped catalyst appeared to be longer, and that methane conversion was higher, than for the undoped catalyst.

In order to confirm this hypothesis, we have compared the catalytic performance for different lengths of catalyst bed over Nd_2O_3 and 50 mol.% SrF_2–Nd_2O_3 under the same flow rate of CH_4–O_2 mixture. For the Nd_2O_3 catalyst, when the catalyst volume was decreased from 0.2 to 0.02 ml, while the GHSV was increased from 20 000 to 200 000 h^{-1}, the catalytic performance remained almost unchanged (Table 3), suggesting that Nd_2O_3 was a very active catalyst which could convert methane efficiently in a short catalyst bed. In contrast, a decrease in methane and oxygen conversions as well as in ethene-to-ethane ratio was found over 50 mol.% SrF_2–Nd_2O_3 catalyst with the same decrease in catalyst volume. This indicated that the reaction zone of the 50 mol.% SrF_2–Nd_2O_3 catalyst bed was longer that that of the Nd_2O_3 catalyst bed, and, with the decrease in reaction zone, the conversions of methane and oxygen would be decreased. It has been accepted that a good OCM catalyst has two functions: (1) the production of methyl radicals and (2) inhibition of the total oxidation of both the methyl radicals and C_2 hydrocarbons.[15] REO, especially La_2O_3 and Nd_2O_3, are very effective at generating methyl radicals; however, these catalysts are also very active for the complete oxidation of these methyl radicals to CO_x.[2,16] The change in surface and bulk properties (*e.g.* surface composition, surface basicity and conductivity) as a result of adding SrF_2 to Nd_2O_3 catalyst resulted in a decrease in the extent of deep oxidation of methyl radicals and C_2 hydrocarbons, leading to an increase in C_2 selectivity. In the next sections, more discussion about this will be presented. Since there is a certain relationship between methane conversion and C_2 selectivity for an oxygen-limited OCM reaction, methane conversion is also found to increase with the improvement in C_2 selectivity. At the same time, with the increase in the length of catalyst bed being exposed to gas-phase oxygen, the chance that ethane will react with surface active oxygen species to produce ethene will increase, leading to an improvement in ethene-to-ethane ratio over 50 mol.% SrF_2–Nd_2O_3 catalyst, as compared with pure Nd_2O_3 catalyst. A similar phenomenon was also found on the BaF_2-promoted REO with variable valence.[17]

Surface composition

The electron binding energies (E_b) and surface composition of the elements on the fresh Nd_2O_3 and 50 mol.% SrF_2–Nd_2O_3 samples are summarized in Tables 4 and 5. In the C 1s spectra, besides the carbon peak due to adventitious carbon at 284.6 eV, another peak was observed at higher energy (289.2 eV) on the pure Nd_2O_3 sample, this corresponds typically to a carbon atom belonging to a carbonate group.[18] The O 1s spectra in the catalyst could be resolved into three peaks located at 531.8, 530.7 and 529.0 eV, respectively (Table 4). The peaks at *ca.* 529.0 eV can be attributed to lattice oxygen (O^{2-}),[19,20] while the other peaks at 531.8 and 530.7 eV cannot be identified because the E_b values of some oxygen species (*e.g.* O^-, OH^-, O_2^{2-}, CO_3^{2-}) fall in the range 530–532 eV. Since the ratio of atomic oxygen concentration to atomic carbon concentration with higher C 1s E_b was much greater than 3 (Table 5), it can be inferred that other oxygen species, *e.g.* OH^-, O^- and O_2^{2-}, may also exist on the catalyst surface besides CO_3^{2-}.[18–22] The Nd $3d_{5/2}$ peak at 982.1 eV can be assigned to Nd^{3+}.[18]

Table 5 Surface composition of various elements on the fresh catalysts

catalyst	atomic concentration, C_x[a] (%)					
	Nd^{3+}	Sr^{2+}	F^-	O^{2-}	other oxygen[b]	C[c]
Nd_2O_3	15.1	—	—	12.5	62.0	10.4
50 mol.% SrF_2–Nd_2O_3	11.4	7.9	5.1	14.0	48.0	13.6

[a] $C_x = (A_x/S_x)/(\Sigma_i A_i/S_i)$, where A = peak area; S = atomic sensitivity factor. [b] Other oxygen refers to the oxygens in CO_3^{2-}, OH^-, O^-, O_2^{2-} *etc.* [c] C does not include adventitious carbon.

After SrF_2 was added to Nd_2O_3 catalyst, the binding energies of the above elements were almost unchanged, but the content of surface carbonate was found to increase, suggesting an increase in the catalyst surface basicity. Sr^{2+} and F^- ions were also detected on the catalyst surface, but the F^- ion content on the surface was apparently lower than that in the bulk. This indicates that F^- ion can easily move into the catalyst bulk. When methane molecules react with surface oxygen species of the catalyst to produce methyl radicals, the methyl radicals may have a chance to react with the adjacent oxygen species and be further deeply oxidized to CO_x species before they desorb from the catalyst surface.[2,3,9–11] Since the fluorine ions cannot react with methyl radicals under the reaction conditions (as proved by the fact that no fluorinated hydrocarbon was detected in the product), the dispersion of inert fluorine ions on the catalyst surface will be beneficial to the isolation of the surface active centres. When one molecule of methane reacts with a surface oxygen species to produce a methyl radical, the chance that this methyl radical reacts continuously with another adjacent oxygen species to produce CO_x will be decreased. This will favour an increase of C_2 selectivity.

Surface basicity

As shown in Fig. 3, one could observe two CO_2 desorption bands, centred at 378 and 675 K, over the Nd_2O_3 catalyst, which were assigned to basic sites with weak and intermediate strengths, respectively. By contrast, two, relatively stronger, CO_2 desorption peaks (the latter appeared at higher temperature) were also observed over 50 mol.% SrF_2–Nd_2O_3 catalyst, suggesting that the surface basicity and basic strength of the catalyst containing strontium fluoride were greater than those of pure Nd_2O_3. This is consistent with the increase in surface carbonate content of the catalyst (XPS result).

Since no carbon dioxide desorption peak was detected on the SrF_2 sample (Fig. 3), the appearance of the new peak at 899 K over 50 mol.% SrF_2–Nd_2O_3 catalyst is obviously related to the interaction between Nd_2O_3 and SrF_2. The peak might arise from the SrO formed as a result of F^- and O^{2-} exchange at high temperature (XRD result, see next section). However, the desorption temperature was much lower than the temperature of $SrCO_3$ decomposition (1613 K),[23] indicating that SrO did not exist as an isolated phase but, rather, was dissolved and highly dispersed in the catalyst. The SrO might exist as a new form in which strontium ion adjoins both fluorine and oxygen ions, *e.g.* (F—Sr—O—Sr—F). Because the electronegativity of fluorine is greater than that of oxygen, its long-distance induced effect will lead to the result that the oxygen ion linking with strontium ion in the catalyst contains fewer negative charges than that in normal strontium oxide and thus, to a decrease in oxide basicity and carbonate decomposition temperature. It is known that most OCM catalysts are basic oxides. Surface basicity was considered by many researchers to be one of the fundamental characteristics of an OCM catalyst for better C_2 selectivity.[8,24–26] However, a very strong basic site will be easily poisoned by the CO_2 generated during the reaction, leading to a higher 'light-off' temperature, or a higher reaction temperature necessary to maintain an adequate level of activity.[24,27,28] Thus, a strong basicity with intermediate basic sites for an OCM catalyst, such as these alkaline-earth-metal fluoride promoted REO catalysts, might be beneficial to obtaining a high C_2 yield at medium temperature.

Bulk composition and structure

XRD indicated that only the hexagonal Nd_2O_3 phase was present in the fresh 25 mol.% SrF_2–Nd_2O_3 catalyst (Fig. 4), the SrF_2 phase could not be found since it dissolves in the Nd_2O_3 phase. However, new phases, such as tetragonal and/or rhombohedral NdOF, were formed in the fresh 50

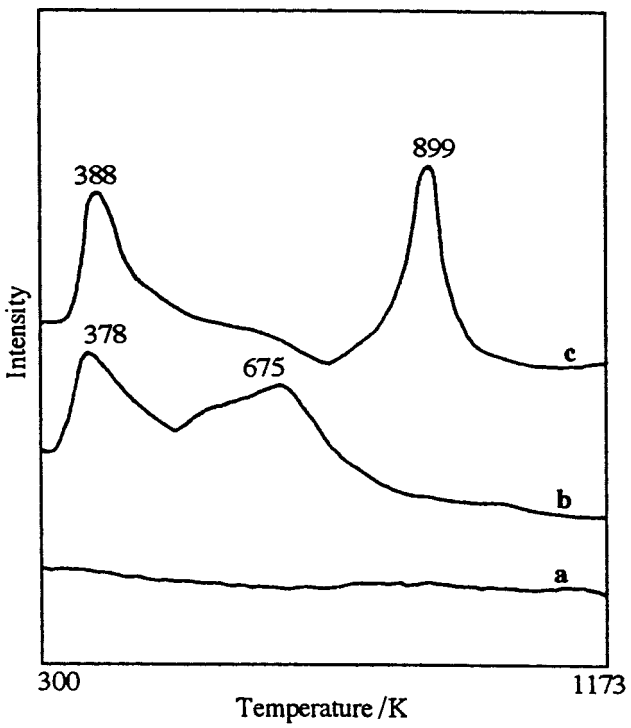

Fig. 3 TPD of CO_2 adsorbed on (a) SrF_2, (b) Nd_2O_3, (c) 50 mol.% SrF_2–Nd_2O_3 catalysts

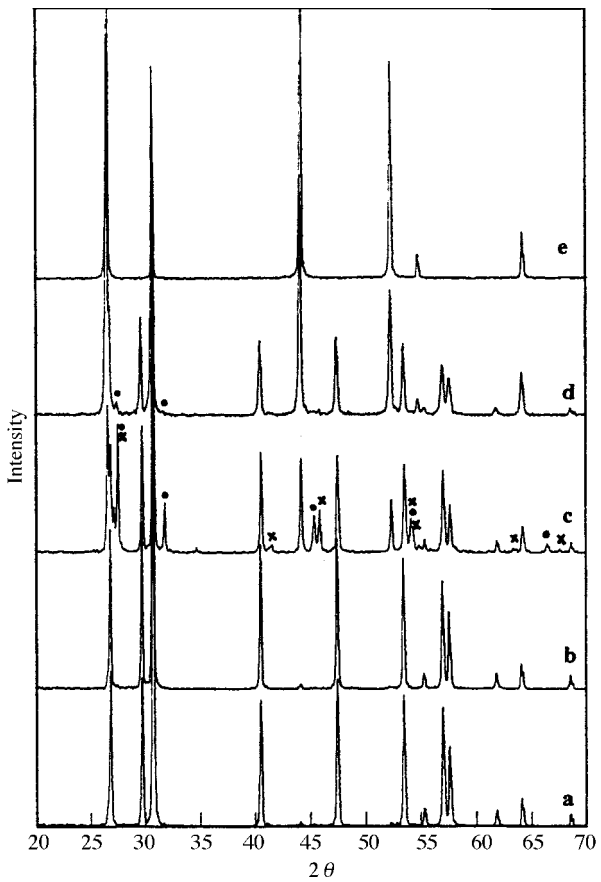

Fig. 4 X-Ray powder patterns of fresh (a) Nd_2O_3 (b)–(d) 25, 50, 80 mol.% SrF_2–Nd_2O_3, (e) SrF_2. (×) Rhombohedral NdOF, (○) tetragonal NdOF.

Table 6 Bulk composition and structure[a] of the fresh 50 mol.% MF_2–Nd_2O_3 (M = Ca, Sr, and Ba) catalysts

catalyst	composition and structure[a]
CaF_2–Nd_2O_3	hexagonal Nd_2O_3(s), tetragonal NdOF(w), cubic CaF_2(w)
SrF_2–Nd_2O_3	hexagonal Nd_2O_3(vs), tetragonal NdOF(m), rhombohedral NdOF(w), cubic SrF_2(s)
BaF_2–Nd_2O_3	hexagonal Nd_2O_3(s), tetragonal NdOF(m), rhombohedral NdOF(m), cubic BaF_2(vs)

[a] vs = very strong; s = strong; m = medium; w = weak.

mol.% and 80 mol.% SrF_2–Nd_2O_3 catalysts, besides cubic SrF_2 and hexagonal Nd_2O_3 phases. This suggests that partial exchange of F^- with O^{2-} took place during the catalyst preparation. The SrO phase formed could not be detected, most probably due to its solution in the catalyst lattice. The content of NdOF reached a maximum in the 50 mol.% SrF_2–Nd_2O_3 catalyst.

The XRD results on different alkaline-earth-metal fluoride promoted neodymium oxide catalysts are summarized in Table 6. Exchange between F^- and O^{2-} also took place and the NdOF phase appeared in the calcined catalysts. The diffraction-line intensity of alkaline-earth-metal fluorides decreased in the order Ba > Sr > Ca in fresh 50 mol.% MF_2–Nd_2O_3 (M = Ca, Sr, and Ba) catalysts. This can be interpreted as follows: as the cationic radii in these alkaline-earth-metal fluorides became increasingly larger than that of Nd^{3+} (0.0995 nm), the solubility of the corresponding fluorides (or oxides) in neodymium oxide or oxyfluoride became smaller and smaller.

The structure of hexagonal Nd_2O_3 can be described by slabs of OLn_4 tetrahedrons linked by three of their edges and forming a complex cationic group $(LnO)_n^{n+}$ separated by ionic oxygens O^{2-},[29] with 17% of 'genetic' oxygen vacancies in the lattice.[30] The tetragonal NdOF can be expressed by the formula LnO_xF_{3-2x} $(0.7 < x \leqslant 1)$,[31,32] the structure of which is closely similar to that of fluorite, the excess F^- ions can be accommodated in a fluorite-like structure and occupy some of the interstitial position as Frenkel defects.[32] Whereas the rhombohedral NdOF is found to be a single phase, whose chemical composition is sharply defined and corresponds exactly to NdOF,[31] this structure is also a slightly distorted CaF_2-type structure. Taking into consideration the fact that many compounds with fluorite-type structure, such as alkaline-earth-metal fluorides, have anion Frenkel defects and anionic vacancies,[33] it is reasonable to postulate that anionic vacancies might also exist in the NdOF lattice with a fluorite-like structure. On the other hand, ionic exchange between the oxide and fluoride phases in the MF_2–Nd_2O_3 (M = Ca, Sr, and Ba) catalysts, as well as the loss of some fluorine (as HF) at high temperature, may also lead to the formation of anionic vacancies and other lattice defects, such as F-centre or O^- species, in order to maintain electroneutrality. The presence of anionic vacancies in the above catalysts will be favourable to the movement of anionic ions as well as to adsorption and activation of O_2 under the reaction conditions.

Conductivity measurement

The conductivity measurement results for Nd_2O_3 and 50 mol.% SrF_2–Nd_2O_3 catalysts are shown in Fig. 5. It is found that, in the temperature region 773–1173 K, the conductivity apparently increases after adding a certain amount of SrF_2 to Nd_2O_3. With increase in temperature, the conductivity of the catalysts increased. According to the Arrhenius equation:

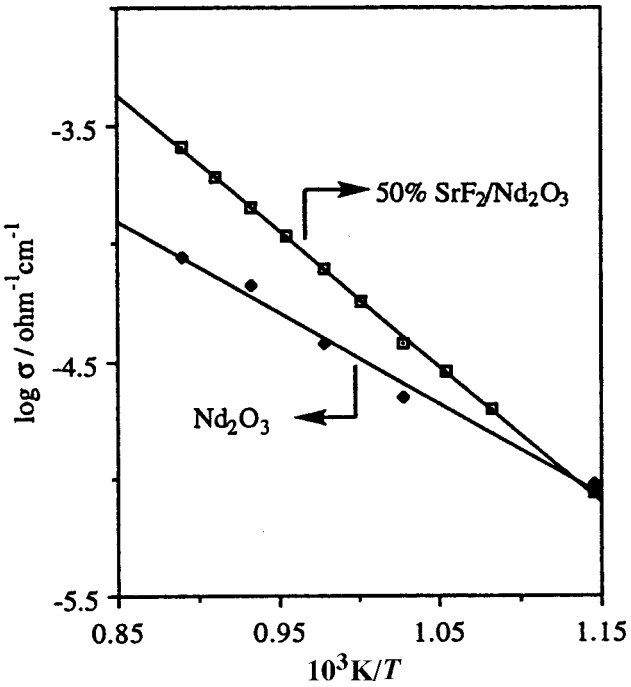

Fig. 5 Effect of temperature on the conductivities of Nd_2O_3 and 50 mol.% SrF_2–Nd_2O_3

$\log \sigma = \log A - 2.303E_a/RT$, the active energy ($E_a$) of conduction can be calculated as follows:

Nd_2O_3

$$\log \sigma = -0.61\text{–}3.88 \times 10^3/T; \quad E_a = 74.3 \text{ kJ mol}^{-1}$$

50 mol.% SrF_2–Nd_2O_3

$$\log \sigma = 1.52\text{–}5.75 \times 10^3/T; \quad E_a = 110 \text{ kJ mol}^{-1}$$

It can be seen that the conduction activation energy of 50 mol.% SrF_2–Nd_2O_3 was also higher than that of pure Nd_2O_3.

Note that the total conductivity of a solid is made up of electron conductivity and ion conductivity, and that ion conduction plays a more important role than electron conduction at high temperature.[34] When a certain amount of SrF_2 was added to Nd_2O_3 catalyst, the increase in conductivity suggests that the mobility of anionic ions in the catalyst increased. This will be favourable to the movement of these species (*e.g.* F^- ion and O^- ion, which might form during the catalyst preparation or under the reaction conditions), which have shown smaller radii and/or fewer negative charges, from the catalyst surface into the bulk. The inference that F^- ion mainly exists in the SrF_2–Nd_2O_3 catalyst bulk has been demonstrated by the above XPS result. Considering the fact that O^- has a higher activity for oxidizing light hydrocarbons than O_2^{2-} and O_2^-,[35] the movement of O^- species from the catalyst surface into the bulk will decrease the chance of deep oxidation of methyl radicals and C_2 hydrocarbons and thus lead to an increase in C_2 selectivity.

Conclusions

The catalytic performance of SrF_2–Nd_2O_3 catalyst was better than that of pure Nd_2O_3 for OCM. The maximum C_2 yield reached 19.6% over 50 mol.% SrF_2–Nd_2O_3 catalyst at 1023 K for $CH_4/O_2 = 3/1$ and GHSV = 20 000 h^{-1}. After the addition of a certain amount of SrF_2 to the Nd_2O_3, the increase in surface basicity and conductivity, as well as the role of F^- on the dispersion of surface active sites, would be favourable to an improvement in C_2 selectivity. Since there is a certain

relationship between methane conversion and C_2 selectivity for an oxygen-limited OCM reaction, methane conversion is also expected to increase with the increase in C_2 selectivity. XRD results indicated that tetragonal and rhombohedral NdOF phases are formed during the catalyst preparation.

This work has been supported by the National Natural Science Foundation of China.

References

1 K. Otsuka, K. Jinno and A. Morikawa, *Chem. Lett*., 1985, 499.
2 K. D. Campbell, H. Zhang and J. H. Lunsford, *J. Phys. Chem*., 1988, **92**, 750.
3 J. H. Lunsford, *Catal. Today*, 1990, **6**, 3.
4 S. Lacombe, C. Geantet and C. Mirodatos, *J. Catal*., 1994, **151**, 439.
5 D. G. Filkova, L. A. Petrov, M. Y. Sinev and Y. P. Tyulenin, *Catal. Lett*., 1992, **13**, 323.
6 R. Burch, G. D. Squire and S. C. Tsang, *Appl. Catal*., 1988, **43**, 105.
7 Y. Amenomiya, V. I. Birss, M. Goledzinowski, J. Galuszka and A. R. Sanger, *Catal Rev. Sci. Eng*., 1990, **32**, 163.
8 A. M. Maitra, *Appl. Catal*., *A*, 1993, **104**, 11.
9 E. Inamatsu and K. Aika, *J. Catal*., 1989, **117**, 416.
10 P. F. Nelson, C. A. Lukey and N. W. Cant, *J. Phys. Chem*., 1988, **92**, 6176.
11 Y. Tong, M. P. Rosynek and J. H. Lunsford, *J. Phys. Chem*., 1989, **93**, 2896.
12 X. P. Zhou, S. Q. Zhou, W. D. Zhang, Z. S. Chao, W. Z. Weng, R. Q. Long, D. L. Tang, H. Y. Wang, S. J. Wang, J. X. Cai, H. L. Wan and K. R. Tsai, *Preprints*, Division of Petroleum Chemistry, American Chemical Society, Washington, DC, 1994, vol. 39, p. 222.
13 R. Long, S. Zhou, Y. Huang, W. Weng, H. Wan and K. Tsai, *Appl. Catal*., *A*, 1995, **133**, 269.
14 M. S. Frant, *Science*, 1966, **154**, 1553.
15 S. J. Korf, J. A. Roos, J. W. H. C. Derksen, J. A. Vreeman, J. G. Van Ommen and J. R. H. Ross, *Appl. Catal*., 1990, **59**, 291.
16 C. H. Lin, K. D. Campbell, J. X. Wang and J. H. Lunsford, *J. Phys. Chem*., 1986, **90**, 534.
17 R. Long, J. Luo, M. Chen and H. Wan, *Appl. Catal*., *A*, 1997, **159**, 171.
18 *Handbook of X-Ray Photoelectron Spectroscopy*, Φ Corporation, 1990.
19 M. S. Hedge and M. Ayyoob, *Surf. Sci*., 1986, **173**, L635.
20 S. Sugiyama, T. Ookubo, K. Shimodan, H. Hayashi and J. B. Moffa, *Bull. Chem. Soc. Jpn*., 1994, **67**, 3339.
21 J. L. Dubois, M. Bisiaux, H. Mimoun and C. J. Cameron, *Catal. Lett*., 1990, 967.
22 M. Ayyoob and M. S. Hedge, *Surf. Sci*., 1983, **133**, 516.
23 R. C. Weast, *Handbook of Chemistry and Physics*, Chemical Rubber Co., Cleveland, OH, 51st edn., 1970–1971, p. B-142.
24 A. M. Maitra, I. Campbell and R. J. Tyler, *Appl. Catal*., *A*, 1992, **85**, 27.
25 V. R. Choudhary and V. H. Rane, *J. Catal*., 1991, **130**, 411.
26 V. D. Sokolovskii, S. M. Aliev, O. V. Buyerskaya and A. A. Davydov, *Catal. Today*, 1989, **4**, 293.
27 H. Mimoun, A. Robine, S. Bonnaudet and C. J. Cameron, *Chem. Lett*., 1989, 2185.
28 J. H. Lunsford, *Natural Gas Conversion II*, Elsevier, Amsterdam, 1994, p. 1.
29 *Handbook on the Physics and Chemistry of Rare Earths*, ed. K. A. Gschneidner, Jr., and L. Eyring, North–Holland, Amsterdam, 1982, vol. 5, ch. 44, p. 322.
30 E. N. Voskresenskaya, V. G. Roguleva and A. G. Anshits, *Catal. Rev. Sci. Eng*., 1995, **37**, 101.
31 K. Niihara and S. Yajima, *Bull. Chem. Soc. Jpn*., 1971, **44**, 643.
32 A. F. Wells, *Structural Inorganic Chemistry*, Oxford University Press, New York, 5th edn., 1984, p. 483.
33 E. Radzhabov, *J. Phys. Condens. Matter*, 1994, **6**, 9807.
34 Z. Zhang, X. E. Verykios and M. Baerns, *Catal. Rev. Sci. Eng*., 1994, **36**, 507.
35 M. Iwamoto and J. H. Lunsford, *J. Phys. Chem*., 1980, **84**, 3097.

Paper 8/00367J; *Received* 13*th January*, 1998